

New potent 5-substituted benzofuroxans as inhibitors of *Trypanosoma cruzi* growth: Quantitative structure–activity relationship studies

Gabriela Aguirre,^a Lucía Boiani,^a Mariana Boiani,^a Hugo Cerecetto,^{a,*}
Rossanna Di Maio,^a Mercedes González,^{a,*} Williams Porcal,^a
Ana Denicola,^b Oscar E. Piro,^c Eduardo E. Castellano,^d
Carlos Mauricio R. Sant'Anna^e and Eliezer J. Barreiro^f

^aDepartamento de Química Orgánica, Facultad de Química-Facultad de Ciencias, Universidad de la República, 11400 Montevideo, Uruguay

^bLaboratorio de Físicoquímica Biológica, Facultad de Ciencias, Universidad de la República, 11400 Montevideo, Uruguay

^cDepartamento de Física, Universidad Nacional de La Plata, 1900-La Plata, Argentina

^dInstituto de Física de São Carlos, Universidade do São Paulo, 13560-São Carlos, Brazil

^eDepartamento de Química, ICE, Universidade Federal Rural do Rio de Janeiro, Seropédica, Brazil

^fLASSBIO, Faculdade de Farmácia, Universidade Federal do Rio de Janeiro, Rio de Janeiro, Brazil

Received 26 May 2005; revised 20 July 2005; accepted 21 July 2005

Available online 3 October 2005

Abstract—Benzofuroxan derivatives have been shown to inhibit the growth of *Trypanosoma cruzi*, the etiological agent of Chagas' disease. Therefore, 2D- and 3D-QSAR models of their in vitro antichagasic activity were developed. Six new derivatives were synthesized to complete a final set of 26 structurally diverse benzofuroxans. The 2D-QSAR model ($r = 0.939$, $r^2_{\text{adj}} = 0.849$) was generated using multiple regression analysis of tabulated substituents' physicochemical properties and indicator variables. In addition, a 3D-QSAR model ($r^2 = 0.997$, $q^2 = 0.802$) was obtained using a comparative molecular field analysis (CoMFA). Due to the well-known benzofuroxan tautomerism, in both approaches (2D- and 3D-QSAR) it was necessary to include an indicator variable to consider the *N*-oxide position (I_6). This parameter was established using low-temperature NMR experiments. Both QSAR models identified the electrophilic character of the substituent α -atom as a requirement for activity. Further support was found using a density functional theory (DFT) approach.

© 2005 Elsevier Ltd. All rights reserved.

1. Introduction

Chagas' disease (CD) or American trypanosomiasis represents a serious public health problem in the countries and zones where it is endemic (21 countries, in Central and South America) because there are no effective methods of immunoprophylaxis or chemotherapy.¹ CD is the illness involving a protozoan organism (*Trypanosoma cruzi*) that maintains 16–18 million people infected and another 100 million at risk. Besides, trypanosomiasis is often the ultimate cause of morbidity for immunocompromised individuals.² The current chemotherapy

against CD, represented by Nifurtimox® (Nfx) and Benznidazole®, is still inadequate.³

These drugs have undesirable side effects and are inefficient in treating chronic CD. So, development of safe and efficient anti-CD drugs continues to be an active area of research. In light of the preceding considerations, our group has been searching for new anti-trypanosomal (against *T. cruzi*) compounds⁴ and has previously described a series of benzo[1,2-*c*]1,2,5-oxadiazole *N*-oxide (benzofuroxan) derivatives that displayed good in vitro activity.⁵ In addition, some aspects related to the mechanism of trypanocidal action of this family of compounds were studied and preliminary structural requirements for adequate activity were established.⁶ To gain further insight into the SAR of benzofuroxan derivatives, herein

* Corresponding authors. Tel.: +598 2 5258618x216; fax: +598 2 525 0749; e-mail addresses: hcerecet@fq.edu.uy; megonzal@fq.edu.uy

we have developed QSAR studies using a conventional methodology as well as a comparative molecular field analysis (CoMFA).⁷ This method, based on ligand–receptor interaction, can be a powerful tool for three-dimensional design of ligand when the receptor site is unrecognized. It was, therefore, expected that QSAR studies might help to delineate the structural requirements for enhanced anti-parasitic activity and thus guide the rational design of new trypanocidal compounds.

To complete a structurally diverse dataset, six new derivatives were synthesized (Chart 1). The biological activity was evaluated in vitro against Tulahuén 2 strain of *T. cruzi* and some potent compounds were obtained.

It is well established that benzofuroxan derivatives exist at room temperature as a mixture of tautomers

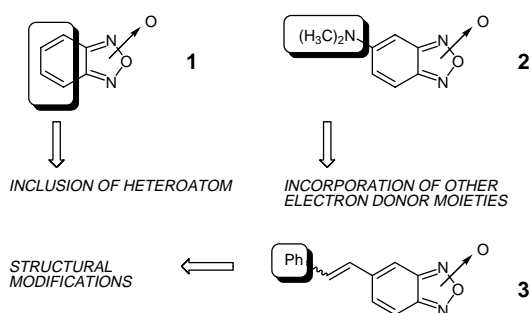


Chart 1. Parent benzofuroxans and structural modifications.

(Fig. 1A). The benzo substituent could occupy the 5- or 6-position and the proportion of both tautomers in the equilibrium depends on the electronic characteristics of the substituent.⁸ In the QSAR studies, we have used the most stable tautomer. To determine the preferential position of the *N*-oxide moiety, temperature-variable NMR studies were carried out.⁹

2. Methods and results

2.1. Synthesis

The aza analogue of derivative **1** (Chart 1), compound **4** (Scheme 1), was prepared as previously described by thermal decomposition of the pyrido[1,2-*d*]tetrazole intermediate.¹⁰ Attempts were made to obtain the amino benzofuroxan **9** to include into the study other mesomeric electron-donor substituents (i.e., NH₂, NHR, Scheme 1).¹¹ Accordingly, the carbamate **8** was synthesized from the acid **5** via the isocyanate **7**. Different reaction conditions were assayed in the deprotection of **8** but none of them afforded the aminobenzofuroxan **9**. So, only compound **8** was obtained as a new derivative possessing a mesomeric electron-donor substituent. Probably, derivative **9** was obtained but in the reaction medium it auto-condensed to produce hydrazine-like compounds, as previously reported.¹² Since olefin **3** (Chart 1) was one of the most potent derivatives previously described, we developed analogues **11–14** using the Bodens-Wittig methodology depicted in Scheme 2.¹³

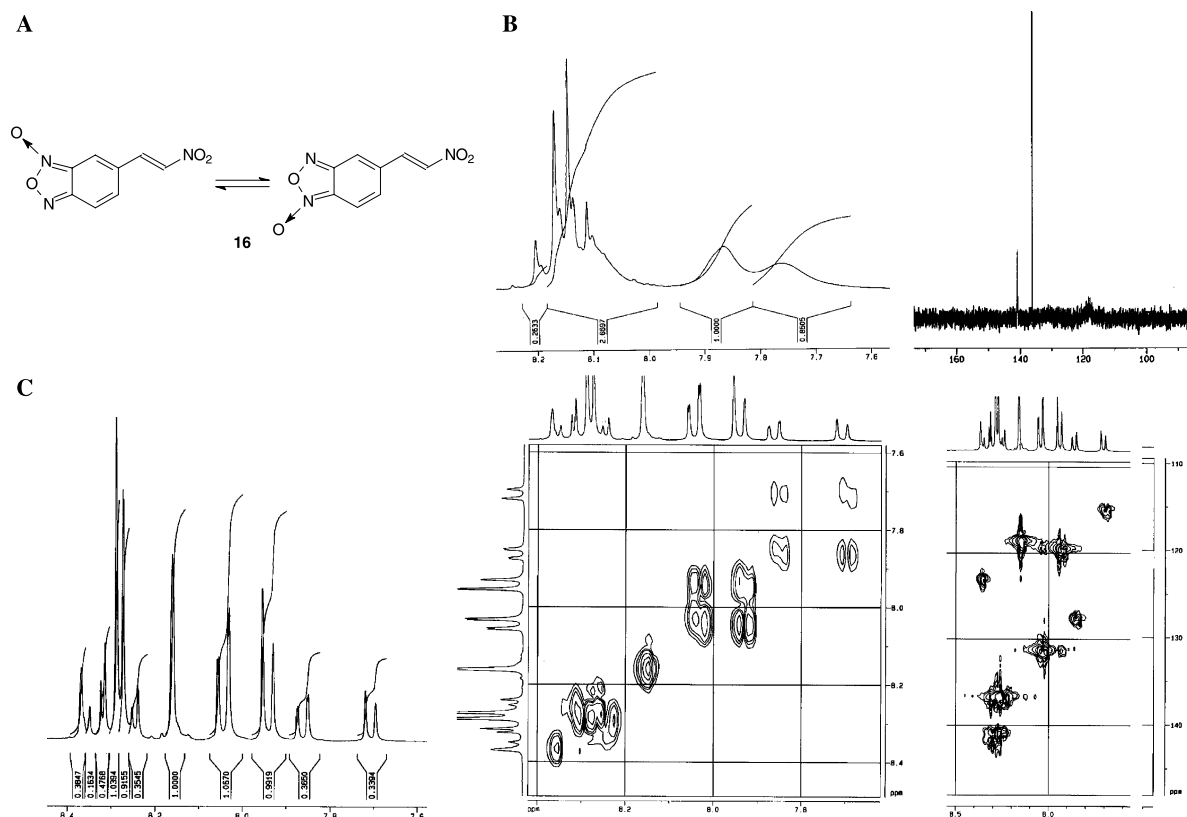
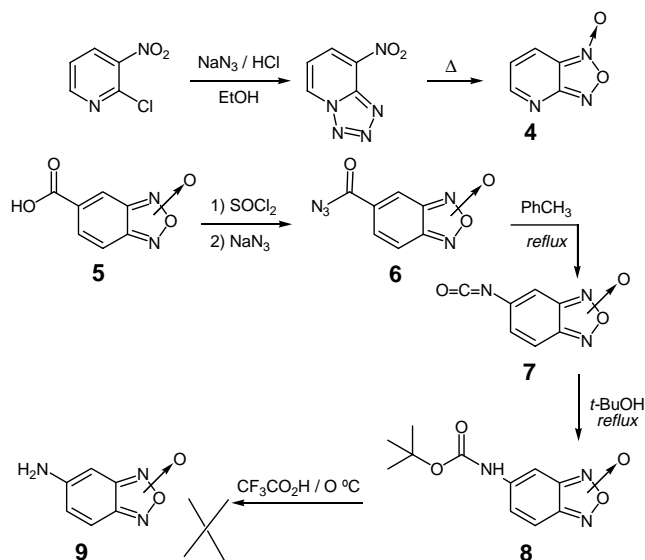


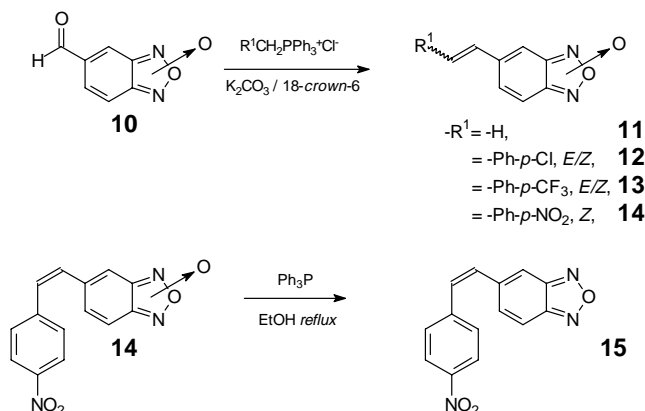
Figure 1. (A) Tautomeric equilibrium of derivative **16**. (B) ¹H and ¹³C NMR spectra of **16** in acetone-*d*₆ at 303 K. (C) ¹H NMR, COSY, and HMQC spectra of **16** in acetone-*d*₆ at 230 K.



Scheme 1. Synthesis of aza-analogue **4** and attempts to synthesize derivative **9** with mesomeric electron-donor substituent.

Derivatives **12** and **13** were obtained as a 50:50 mixture of *E* and *Z* isomers. While, the reaction between **10** and 4-nitrobenzyltriphenylphosphonium bromide yielded only the *Z* isomer, namely **14**. The stereochemistry around the olefinic system was established using the ¹H NMR coupling constants. To study the effect of the *N*-oxide moiety on the activity displayed by these derivatives, we synthesized derivative **15**, the deoxygenated derivative of one of the most active compounds (**14**). Derivative **15** was prepared by reaction of **14** with triphenylphosphine in boiling ethanol (Scheme 2).¹⁴

At room temperature (303 K) ¹H and ¹³C NMR spectra of the benzofuroxans showed broad signals due to tautomeric equilibrium (i.e., Fig. 1A). When NMR experiments were carried out at low temperature (e.g., 233 K), the aromatic region showed narrow peaks corresponding to both tautomers (Figs. 1B and C).⁹ In acetone solution, (approximately 10% w/v) at 303 K, compound **16** shows broad resonance signals due to incomplete



Scheme 2. Synthesis of analogues of benzofuroxan **3** and deoxy derivative **15**.

coalescence (Fig. 1B). While, on cooling, the broad signals were resolved below 263 and at 230 K it was possible to record the complete series of spectra (¹H, ¹³C NMR, and HMQC, HMBC, and COSY experiments, Fig. 1C). Hence, the ratio of 5- and 6-isomers was determined at low temperature (Table 1).

All new compounds were identified by IR, MS, ¹H NMR, ¹³C NMR, COSY, and HETCOR experiments, and their purity established by TLC and microanalysis.

2.2. Biological characterization

2.2.1. Anti-trypansomal activities. All compounds were tested in vitro against *T. cruzi*. Epimastigote forms of *T. cruzi*, Tulahuen 2 strain, were grown in axenic media as described in Section 5. The compounds were incorporated into the media at 25 μM and their ability to inhibit the parasite growth was evaluated in comparison to the control (no drug added) (Table 2). Nfx was used as the reference trypanocidal drug. Growth of the parasite was followed by measuring the increase in absorbance at 600 nm, which had previously been shown to be proportional to the number of cells present.¹⁵ The percentage of inhibition was calculated as follows: % = {1 - [(A_p - A_{0p})/(A_c - A_{0c})]} × 100, where A_p is A₆₀₀ of the culture containing the drug at day 5; A_{0p} is A₆₀₀ of the culture containing the drug right after addition of the inocula (day 0); A_c is A₆₀₀ of the culture in the absence of any drug (control) at day 5; A_{0c} is A₆₀₀ in the absence of the drug at day 0. The IC₅₀ concentration (50% inhibitory concentration) was determined for compounds presenting high trypanocidal activity (Fig. 2).

2.3. Quantitative structure–activity relationship studies

The 21 benzofuroxans used in the 2D-QSAR study were **8** and the previously described derivatives **1–3**, **5**, **10**, and

Table 1. ¹H NMR data at low temperature

Compound	-R	Temperature (K) ^a /solvent	6-Tautomer/5-tautomer ratio
16	-E-CH=CHNO ₂	230/CD ₃ COCD ₃	2.90
17	-NO ₂	233/CDCl ₃	2.70
10	-CHO	233/CDCl ₃	1.90
18	-CH=NOH	233/CD ₃ COCD ₃	1.60
3	-E-CH=CHPh	233/CDCl ₃	1.38
19	-CH ₂ I	233/CDCl ₃	1.33
20	-CH ₂ Cl	233/CDCl ₃	1.02
21	-CH ₂ OH	263/CD ₃ COCD ₃ ^b	1.00 ^b
22	-Ph	243/CDCl ₃	0.95 ^c
23	-CH ₃	227/CDCl ₃ ^d	0.92 ^d
24	-OCH ₃	248/CDCl ₃	0.56

^a Conditions used in NMR experiments.

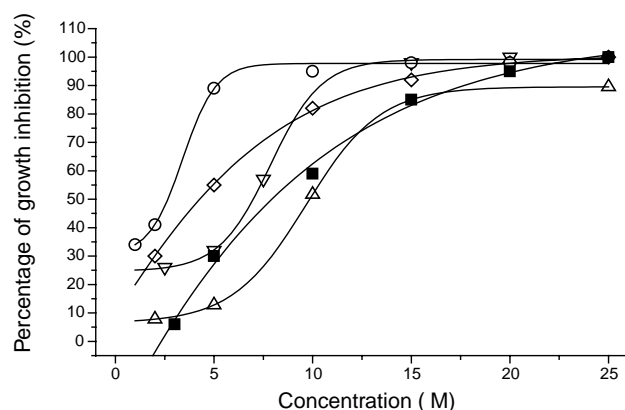
^b Data taken from Ref. 9a.

^c Ratio was estimated since signals were not resolved.

^d Data taken from Ref. 8c.

Table 2. In vitro activity of benzofuroxan derivatives and Nfx on *T. cruzi* (Tulahuen strain) at 25 μ M

Compound	Growth inhibition (%) ^{a,b}
Nfx	100.0
4	53.0
6	34.0
7	8.0
8	18.0
11	31.0
12	100.0
13	89.0
14	96.0
15	18.0

^a Growth inhibition of epimastigotes at day 5.^b The results are means of three different experiments with a SD less than 10% in all cases.**Figure 2.** Dose–response of selected benzofuroxan derivatives as anti-*T. cruzi* agents, **Z-3** (▽), **12** (◇), **13** (△), **16** (○), and Nfx (■). 50% Inhibitory dose (IC₅₀, μ M) for selected derivatives.

16–30 (Table 3).⁵ Compounds **4** and **11–14** were not included since their substituent physicochemical properties are not tabulated.¹⁶

Twenty-six benzofuroxans, **1–5**, **8**, **10–14**, and **16–30**, were employed in the CoMFA study. The dataset was divided into a training set and a test set.

Taking into account the tautomeric equilibrium of the benzofuroxan system, an indicator variable (I_6) was introduced that showed the preferential position of the *N*-oxide moiety (Fig. 1). The I_6 variable was estimated from low-temperature NMR experiments (Table 1). It takes a value of 1.0 when the substituent is preferentially 6-positioned (6-tautomer/5-tautomer ratio < 1.50), it takes a value of 0.0 when it is preferentially 5-positioned (6-tautomer/5-tautomer ratio < 1.00), and it takes a value of 0.5 when in the equilibrium exists similar quantities of both tautomers (1.50 \geq 6-tautomer/5-tautomer ratio \geq 1.00) (Table 1).

For derivatives not examined by NMR experiments, the I_6 variable was assigned according to electronic characteristics of substituents (Table 3). For derivative **4** it took the value of 1.0¹⁰ and for derivatives **11–14** it took the value of 0.5 as the parent compound **3** (Chart 1). The

biological activity was expressed as the percentage of growth inhibition (% GI) at day 5 and at 25 μ M with respect to untreated control. The benzofuroxans were carefully selected to avoid the introduction of artifact in the correlations (we exclude absolute 0% and absolute 100%). As the dependent variable in the linearization procedure, we used \log_{10} (% GI) values, shown in Table 3.¹⁷ In the equations and models, n represents the number of data points, r^2 is the correlation coefficient, s is the standard deviation of the regression equation, and r^2_{adj} defines the cross-validated correlation coefficient. For the CoMFA models, q^2 represents the leave-one-out cross-validated r^2 value, SEE defines the standard error of estimate, SEP defines the standard error of prediction, and the F value is related to the F statistic analysis (Fischer test).

In the 2D-QSAR analysis, we used the previously tabulated substituents constants related to the electronic, the lipophilic, and the steric properties (Hammett constants σ_m , σ_p , and σ^- , Swain-Lupton's constants \mathcal{F} and \mathcal{R} , lipophilic constant π , and molar refractivity MR).¹⁶ Two indicator variables, I_{HBD} (hydrogen bond donor) and I_{HBA} (hydrogen bond acceptor), were also included to account for hydrogen bonding ability of the substituent. I_{HBD} or I_{HBA} takes a value of 1 if the substituent acts as hydrogen bond donor or acceptor and zero otherwise.¹⁶

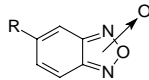
One-variable and multivariable regressions between the activity and the physicochemical descriptors were studied and the best equation was obtained with the independent variables \mathcal{F} , MR, I_{HBD} , and I_6 ($r = 0.879$, $r^2_{adj} = 0.711$, and $s = 0.254$). However, the activity of derivative **26** was poorly predicted by this correlation (predicted \log_{10} (% GI) = 1.57). This fact could be indicating that these independent variables did not correctly describe the biological behavior of this compound, so it was omitted from the study. Hence, by omitting derivative **26** a best correlation was obtained, with an improvement in the statistical parameters (Eq. (1), Fig. 3).

$$\log_{10}(\% \text{ GI}) = 1.31(\pm 0.10) + 1.0(\pm 0.1)I_6 + 0.15(\pm 0.04)MR - 1.31(\pm 0.24)F - 0.51(\pm 0.09)I_{HBD} \quad (1)$$

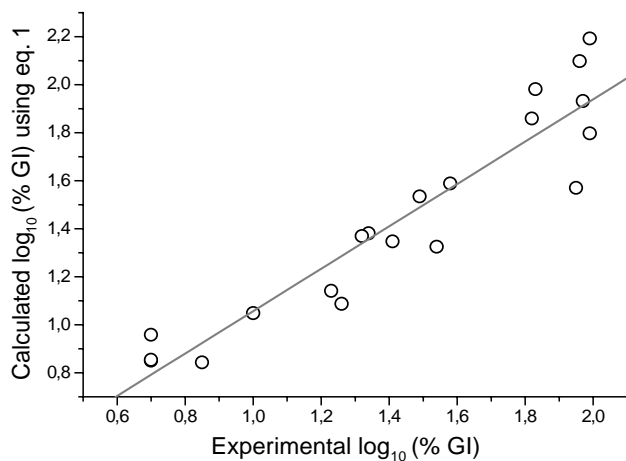
$$n = 20, r = 0.939, r^2_{adj} = 0.849, s = 0.184, \text{ and } p < 0.0001$$

Besides, the correlation matrix for the used physicochemical descriptors was performed and cross-correlations between the descriptors were not obtained.¹⁸ Thus, these parameters are orthogonal, allowing its safe use in the multilinear regression.¹⁹

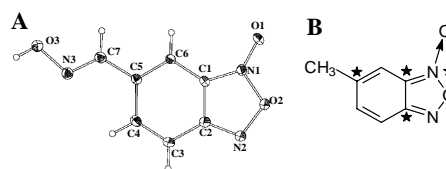
3D-QSAR analysis was performed using the CoMFA module implemented in SYBYL 6.9 package.²⁰ Molecules were built using crystallographic data of derivative **18** (Fig. 4A) to constrain furoxan ring bond lengths and angles. For systems in which no information exists about the binding site, it is a well-established assumption to consider that a similar class of molecules (congeneric series) binds to the putative receptor site

Table 3. Benzofuroxan derivatives and substituent descriptors used to derive Eq. (1) of the 2D-QSAR model


Compound	–R	log ₁₀ (% GI) ^a	I ₆ ^b	MR ^c	<i>F</i>	I _{HBD}
1	–H	1.54	0	0.10	0.00	0
2	–N(CH ₃) ₂	1.41	0	1.56	0.15	0
3	– <i>E</i> -CH=CH-Ph	1.99	0.5	3.42	0.10	0
5	–CO ₂ H	0.70	0.5	0.69	0.34	1
8	–NHCO ₂ C(CH ₃) ₃	1.26	0	3.05 ^f	0.13	1
10	–CHO	1.83	1	0.69	0.33	0
16	– <i>E</i> -CH=CH-NO ₂	1.96	1	1.64	0.35	0
17	–NO ₂	1.95	1	0.74	0.65	0
18	–CH=NOH	1.58	1	1.03	0.28	1
19	–CH ₂ I	1.97	0.5	1.86	0.12	0
20	–CH ₂ Cl	1.99	0.5	1.05	0.13	0
21	–CH ₂ OH	1.32	0.5	0.72	0.03	1
22	–Ph	1.49	0	2.54	0.12	0
23	–CH ₃	1.34	0	0.56	0.01	0
24	–OCH ₃	1.00	0	0.79	0.29	0
25	–CH=C(CN) ₂	1.82	1	1.97	0.57	0
26	–CN	0.95	1	0.63	0.51	0
27	–CH=NNHC(S)NH ₂	1.23	0.5	2.96	0.46	1
28	–SO ₂ NH ₂	0.85	0.5	1.23	0.49	1
29	–Cl	0.70	0	0.60	0.42	0
30	–Br	0.70	0	0.89	0.45	0

^a % GI: percentage of *T. cruzi* growth inhibition at 25 μM.^b I₆: indicator variable that takes value 1 when the substituent is preferentially 6-positioned with respect to *N*-oxide moiety, value 0 when it is preferentially 5-positioned and value 0.5 when in equilibrium there exists an equal quantity of 5- and 6-positioned tautomers at low temperature.^c To autoscale the independent variables, the MR reported is MR_{lit}/10, being MR_{lit} the value taken from Ref. 16b.**Figure 3.** Actual versus calculated activity from the 2D-QSAR model (Eq. (1)).

adopting a similar geometry and orientation. This was done by RMS fitting of the atoms to the template molecule compound **23**, a 6-alkyl derivative, as indicated in Figure 4B. For the complete CoMFA details, see Section 5. Lipophilic properties of the compounds were included into the analyses, as cLog *P* (Log *P* calculated by Ghose-Crippen method).²¹ Only models having a value of *q*² above 0.5 were considered (Table 4). It is widely accepted that a correlation with a *q*² value greater than 0.5–0.6 is useful for the prediction of new biologically active molecules.²²

**Figure 4.** (A) ORTEP²³ molecular plot of derivative **18** at 120 K showing the labeling of the non-H atoms and their displacement ellipsoids at the 30% probability level. (B) Molecule **23**, used as template molecule in the CoMFA studies. Starred atoms were the ones used for superimposition.

It is remarkable that no 3D-QSAR model could be derived without using the indicator variable of localization of the *N*-oxide moiety (*I*₆), something previously seen in the 2D-QSAR study. Model I (1–3, 5, 10, 16, 18–21, and 23–30) is the only one that includes a lipophilicity parameter (c Log *P*), but with a very low contribution. This is in agreement with 2D-QSAR where no contribution of the *π* parameter was found. Model II was obtained when halide derivatives **19** and **20** were excluded, a subject that would be discussed further below, and voluminous compounds **8** and **22** incorporated. Models II–VII were quite similar, being the electrostatic term always the most important. The best model (model IV), according to the number of components (5) and the number of data points used (22), presented similar steric, electrostatic, and indicator variable (*I*₆) contributions as the model with the best *r*² and *q*² (model VII). The model VII, generated using 20 molecules (1–5, 11–12, 14, 16,

Table 4. Summary of CoMFA results

CoMFA model	PLS analysis						Contribution				<i>n</i>
	<i>q</i> ²	Components	SEP	<i>r</i> ²	SEE	<i>F</i> value	Steric	Electrostatic	Other variables		
									<i>I</i> ₆	c Log <i>P</i>	
I	0.559	6	0.392	0.974	0.096	69.44	—	65 ^a	26	9	18
II	0.620	6	0.329	0.989	0.055	169.34	26 ^b	57 ^b	17	—	18
III	0.667	6	0.310	0.991	0.055	215.79	25 ^c	63 ^c	12	—	19 ^c
IV	0.680	5	0.286	0.981	0.070	164.92	33 ^d	57 ^d	10	—	22 ^f
V	0.712	6	0.289	0.992	0.049	279.18	31 ^c	57 ^c	12	—	21 ^g
VI	0.753	6	0.271	0.994	0.040	343.21	32 ^c	58 ^c	10	—	20 ^h
VII	0.802	8	0.266	0.997	0.031	492.45	30 ^c	59 ^c	11	—	20 ⁱ

^a Contribution truncated to: ± 5 kcal/mol.^b Contribution truncated to: ± 10 kcal/mol.^c Contribution truncated to: ± 30 kcal/mol.^d Contribution truncated to: ± 20 kcal/mol.^e Compounds used in model II (see text) and derivative **4**.^f Compounds used in model III and derivatives **11–13**.^g Compounds used in model IV without derivative **8**.^h Compounds used in model V without derivative **10**.ⁱ Compounds used in model VI without derivative **13** and with derivative **14**.**Table 5.** Test set predicted log₁₀ (% GI) from CoMFA model VII

Compound	Observed log ₁₀ (% GI)	Predicted log ₁₀ (% GI) ^a
8	1.26	0.70
10	1.83	1.39
17	1.95	1.06
19	1.97	1.14
20	1.99	1.31

^a CoMFA predicted biological activity ($r = 0.800$, $s = 0.186$).

18, and **21–30**) with lower SEE (0.031) and SEP (0.266), was selected as the best model to explain the SAR and to carry out further analysis. The steric, electrostatic, and indicator variable (I_6) contributions to model VII were 30:59:11. The model VII predicted activities for the test set (derivatives **8**, **10**, **17**, **19**, and **20**) are shown in Table 5. To visualize the CoMFA results, the CoMFA contour maps were created by using the data from the PLS analysis of model VII. The steric contour maps are shown as green and yellow polyhedra in Figure 5A, with the green ones sterically favored regions and the yellow ones indicating sterically disfavored regions. The green polyhedra may be envisioned as hydrophobic cavities in some receptor, which can accommodate hydrophobic groups. In contrast, the yellow polyhedra may represent areas already occupied by the receptor. The electrostatic contour maps (Fig. 5B) also illustrate with red polyhedra

the areas in which groups with increased negative charge are associated with increased biological activities. This can be envisioned as electropositive groups within the active pocket of some biological receptor. In contrast, the blue contours can be visualized as the electronegative groups in the active pocket of the biological receptor and indicate where positively charged groups in the benzofuroxans could improve biological activity.

The CoMFA electrostatic map superimposed on the structure of one of the most active compounds (**3**, Fig. 5B) shows a positive electrostatic contour plot around the substituent's α -atom, pointing to this atom as a possible electrophilic center. These facts, along with the important electrostatic contribution in all the CoMFA models (ca. 60%), prompted us to study the possible participation of this center in a biochemical reaction such as that shown in Figure 6. If this center acts as an electrophilic reactant, then a biological nucleophile, i.e., thiol group, could be covalently bonded to it and this reaction could be implicated in cellular toxic effects.

To further assess this possibility, the LUMO energy (E_{LUMO}), global hardness (η) ($(E_{\text{LUMO}} - E_{\text{HOMO}})/2$), electrostatic-fit atomic charges (EP) on substituent α -atom, and substituent α -atomic orbital coefficients of the LUMO ($\text{LUMO}_{\text{coeff}}$)²⁴ were determined using the densi-

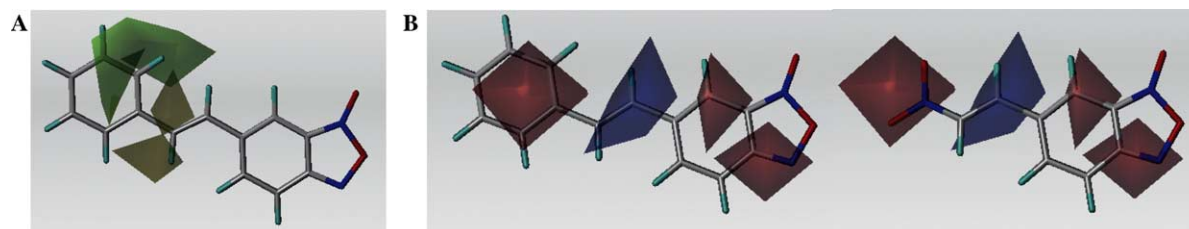


Figure 5. (A) CoMFA steric map superimposed on the structure of compound **3** (model VII contoured at 0.075 and -0.075 levels). (B) CoMFA electrostatic map superimposed on the structure of compounds **3** and **16** (model VII contoured at 0.075 and -0.075 levels).

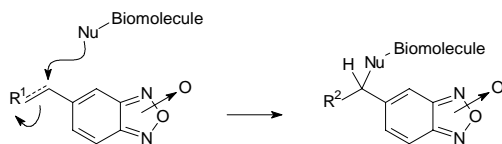


Figure 6. Speculative mechanism of action for the most active benzofuroxans.

ty functional theory (DFT). The selected molecules were built as indicated above and geometries were optimized with the semi-empirical molecular orbital method, MNDO, as implemented in the Spartan'04, 1.0.1 version, suite of programs.²¹ The orbital population analysis was obtained through a single point calculation using the density functional methodology B3LYP/6-31G*.²⁵ Compounds were divided into two groups, actives (% GI ≥ 50) and inactive (% GI < 50), according to biological activity. The difference in electronic properties between groups was analyzed using a nonparametric test (Mann–Whitney *U* test) (Table 6). The LUMO energy was the only variable statistically different at the 0.01 level (Fig. 7A). While the LUMO_{coeff} of substituent α -atom were not statistically different, some clustering may be envisaged (Fig. 7B). The other two studied variables (EP charge and η) became not significantly different, at the 0.01 level, for both pre-defined populations of compounds.

3. Discussion

The new analogues of compound **3** (**12–14**) showed excellent anti-trypanosomal activity, being derivative **12** the best one. The absence of a phenyl moiety, derivative **11**, led to a complete loss of activity. The aza analogue **4** resulted in being more active than the parent compound **1** (53% growth inhibition at 25 μ M for **4** versus 35% for **1**). The aza substitution could be a structural motif to include in future chemical modifications.

Derivative **8** confirmed previous results from other inactive benzofuroxans with mesomeric electron-donor substituents. Such as in previous reports,^{5,26} the absence of the *N*-oxide moiety led to inactive compounds, confirming that this group is playing a role in the mechanism of benzofuroxans' trypanosomal toxicity (compare the activity of derivative **14** with that of deoxy-derivative **15**, Table 2).

The 2D- and 3D-QSAR developed models were completely coincident regarding benzofuroxan structural requirements for an adequate activity. Besides, both analyses resulted in becoming complementary. It is clear that the position of the *N*-oxide moiety in benzofuroxans plays an important role in the activity, since all QSAR models included the indicator variable (*I*₆). Moreover, 2D-QSAR results indicate the relevance of substituent volume in the bio-response and 3D-QSAR data showed favorable contour maps at the end of the substituent. A negative-charge-favored region over the substituent's end, in the active compounds (**3**, and **12–14**) a phenyl group, could be interpreted as a π interaction with an electropositive group in a possible receptor, such as a π -stacking or cation- π interaction. These negative regions generated by CoMFA overlapped with the nitro moiety in derivative **16** (red zone in Fig. 5B), one of the most active benzofuroxans developed at the moment. The blue contour (positive-charge-favored region), occurring on the substituent's α -carbon, could be indicative of a mechanism of action related to a covalent bond formation process (nucleophile–electrophile interaction). Complementary information was obtained from 2D-QSAR studies, where the substituent's electronic effect was related to the activity. An inductive electron-withdrawing group decreased activity (see derivative **26** with $\rho = 0.51$), whereas an inductive electron-donor group increased activity (see derivative **3** with $\rho = 0.10$). Finally, according to 2D-QSAR substituents able to act as hydrogen bond donors lead to activity loss (see derivatives **5**, **8**, **18**, **21**, **27**, and **28**).

Table 6. Electronic properties and statistical analysis of two populations of benzofuroxans (actives, upper side and inactive, lower side)

Compound	log (% GI)	<i>E</i> _{LUMO} (eV)	η^a (eV)	EP charge ^{a,b}	LUMO _{coeff} ^{a,c,d}
3	1.99	−2.45	1.6	−0.251	0.016
20	1.99	−2.57	1.8	0.022	0.006
19	1.97	−2.55	1.8	−0.960	0.028
16	1.96	−3.31	1.6	−0.119	0.077
17	1.95	−3.41	1.7	1.018	—
10	1.83	−3.10	1.7	0.635	0.061
25	1.82	−3.67	1.6	−0.254	0.124
18	1.58	−2.42	1.7	0.132	0.008
22	1.49	−2.44	1.7	0.096	—
11	1.49	−2.43	1.7	−0.188	0.006
21	1.32	−2.32	1.8	−0.075	0.005
31	1.00	−2.34	1.8	−0.173	0.026
5	0.70	−2.29	1.7	0.980	0.029

^a At the 0.01 level, the two means are not significantly different.

^b Substituent α -atom EP charge in atomic units.

^c Substituent α -atom LUMO_{coeff} in atomic units.

^d The means of the two datasets of activities at the 0.105 level are significantly different (*t* test, mean_{active} = 0.052, mean_{inactive} = 0.015, *t* = −1.81, *p* = 0.1046).

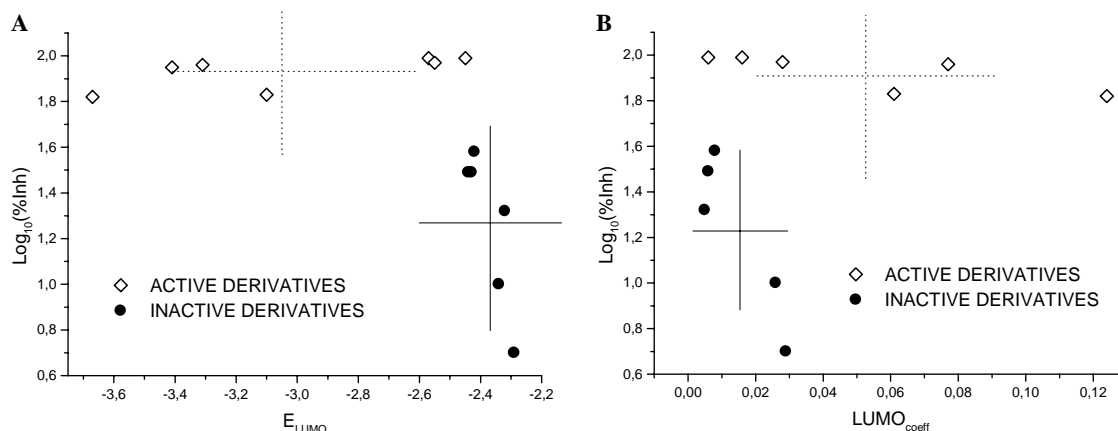


Figure 7. (A) Distribution of E_{LUMO} and activity for the benzofuroxan derivatives selected for t test analysis. (B) Distribution of $\text{LUMO}_{\text{coeff}}$ and activity for the benzofuroxan derivatives selected for t test analysis.

The two-population analysis gave further support to the tentative mechanism depicted in Figure 6. For the studied compounds, active derivatives had lower E_{LUMO} (E_{LUMO} means = -3.01 eV) values than the corresponding energies for the studied inactive compounds (E_{LUMO} means = -2.37 eV), implying that reaction with a nucleophile would be kinetically more favorable for the first group. While, atomic contribution at the substituent α -atom to the LUMO points in the same direction, no statistically relevant difference between groups was found. Evidently, as it was demonstrated by the 2D- and 3D-QSAR models, other characteristics of the molecules are relevant for activity (donor hydrogen bond capacity, volume, and presence of N -oxide moiety) apart from electrophilicity.

Overall, we have developed robust 2D- and 3D-QSAR models that not only explain the variance in biological activities of a set of specific benzofuroxan inhibitors of growth of *T. cruzi* but also correlate between each other.

4. Conclusions

New benzofuroxan derivatives with potent inhibitory activity in vitro against *T. cruzi* are described. Statistically valid 2D- and 3D-QSAR models were developed using a set of twenty-six antitrypanosomal benzofuroxans. Both models showed the importance of electronic properties and more specifically of the electrophilic character of the molecules for the anti-*T. cruzi* activity. Active compounds are good electrophiles and the substituent α -carbon may be considered a possible center of reaction. While lipophilicity was not related to activity, the volume of the substituent was relevant. This volume was also associated with negative electrostatic regions 7–10 Å away from the N -oxide moiety which could be related to aromatic π interactions.

In the absence of any knowledge about the target of these benzofuroxans, the final 2D-QSAR and CoMFA models provide a guide for the design of potentially more active and potent analogues.

5. Experimental

5.1. Chemistry

All starting materials were commercially available research-grade chemicals and used without further purification. Compounds **4–8** and **10** were prepared according to the literature.^{10,11} All solvents were dried and distilled prior to use. All the reactions were carried out in a nitrogen atmosphere. The typical work-up included washing with brine and drying the organic layer with sodium sulfate. Melting points were determined with a Leitz Microscope Heating Stage Model 350 apparatus and are uncorrected. Elemental analyses were obtained from vacuum-dried samples (over phosphorous pentoxide at 3–4 mm Hg, 24 h at room temperature) and performed on a Fisons EA 1108 CHNS-O analyzer and were within $\pm 0.4\%$ of theoretical values. Infrared spectra were recorded on a Perkin-Elmer 1310 apparatus, using potassium bromide tablets for solid and oil products; the frequencies are expressed in cm^{-1} . ^1H NMR and ^{13}C NMR spectra were recorded on a Bruker DPX-400 (at 400 and 100 MHz) instrument, with tetramethylsilane as the internal reference and in the indicated solvent; the chemical shifts are reported in ppm. The ^1H and ^{13}C NMR signals reported were obtained at room temperature. Bruker software was used to perform NOE, COSY, HMQC, and HMBC experiments. Mass spectra were recorded on a Shimadzu GC-MS QP 1100 EX instrument, for electronic impact at 70 eV and 20 eV or chemically ionized with methane.

5.1.1. N^1 -Oxidepyrido[2,3-*c*]1,2,5-oxadiazole (4**).** ^1H NMR (acetone- d_6 , 400 MHz): δ 7.48 (m, 1H), 8.07 (m, 1H), 8.90 (m, 1H); ^{13}C NMR (acetone- d_6 , 100 MHz): δ 122.83, 125.52, 129.37, 161.07; MS, m/z (abundance): 137 (M^+ , 63%), 121 (5%), 107 (49%). Anal. ($\text{C}_5\text{H}_3\text{N}_3\text{O}_2$) C, H, N.

5.1.2. General procedure for the synthesis of derivatives 11–14. A mixture of aldehyde **10** (100 mg, 1 equiv), the corresponding phosphonium salt (methyltriphenylphosphonium iodide, 4-chlorobenzyltriphenylphosphonium chloride, 4-trifluoromethylbenzyltriphenylphosphonium

chloride, and 4-nitrobenzyltriphenylphosphonium bromide) (1.1 equiv), K_2CO_3 (1.1 equiv), 18-crown-6 (0.01 equiv), and THF (3.0 mL) as solvent was stirred at reflux until the carbonyl compounds were not present (SiO_2 , petroleum ether/EtOAc (8:2)). The solvent was evaporated in vacuo, the residue was treated with brine (5.0 mL) and extracted with EtOAc (3 \times 10.0 mL). After the work-up, the organic solvent was evaporated under reduced pressure. The residue was purified by column chromatography (SiO_2 , petroleum ether/EtOAc (9:1)).

5.1.2.1. 5-(Ethenyl)- N^1 -oxidebenzo[1,2-*c*]1,2,5-oxadiazole (11). Brown solid (58 mg, 60%); mp 55.9–58.5 °C; IR ν_{max} 3090, 1616, 1576, 990, 926 cm^{-1} ; 1H NMR ($CDCl_3$, 400 MHz): δ 5.52 (m, 1H), 5.59 (m, 1H), 6.75 (m, 1H), 7.50 (br s, 3H); MS, m/z (abundance): 162 (M^+ , 100%), 146 (18%), 116 (8%), 102 (71%). Anal. ($C_8H_6N_2O_2$) C, H, N.

5.1.2.2. 5-[2*E*/*Z*-(4-Chlorophenyl)ethenyl]- N^1 -oxidebenzo[1,2-*c*]1,2,5-oxadiazole (12). Yellow solid (98 mg, 60%); mp 96.6–98.0 °C; IR ν_{max} 1611, 1522, 957, 843, 689 cm^{-1} ; 1H NMR ($CDCl_3$, 400 MHz): δ 6.79 (d, J = 12.0 Hz, 0.5H), 6.90 (d, J = 12.0 Hz, 0.5H), 7.19 (br s, 0.5H), 7.34 (s, 2H), 7.43 (d, J = 16.0 Hz, 0.5H), 7.46 (d, J = 8.5 Hz, 1H), 7.40–7.50 (br s, 2H), 7.54 (d, J = 16.0 Hz, 0.5H), 7.70 (d, J = 8.5 Hz, 1H), 7.88 (br s, 0.5H); MS, m/z (abundance), 2*E*: 272 (M^+ , 100%), 256 (24%), 226 (8%), 212 (64%), 177 (46%), 149 (9%); 2*Z*: 272 (M^+ , 100%), 256 (21%), 226 (9%), 212 (77%), 177 (63%), 149 (24%). Anal. ($C_{14}H_9ClN_2O_2$) C, H, N.

5.1.2.3. 5-[2*E*/*Z*-(4-Trifluoromethylphenyl)ethenyl]- N^1 -oxidebenzo[1,2-*c*]1,2,5-oxadiazole (13). Orange solid (95 mg, 52%); mp 58.0–59.5 °C; IR ν_{max} 1612, 1574, 1525, 1323, 960, 848, 700 cm^{-1} ; 1H NMR ($CDCl_3$, 400 MHz): δ 6.70 (d, J = 12.2 Hz, 0.5H), 6.87 (d, J = 12.2 Hz, 0.5H), 7.01 (br s, 0.5H), 7.18 (d, J = 16.0 Hz, 0.5H), 7.25 (d, J = 16.0 Hz, 0.5H), 7.30–7.40 (br s, 2H), 7.35 (d, J = 8.0 Hz, 1H), 7.57 (d, J = 8.0 Hz, 1H), 7.60 (br s, 0.5H), 7.65 (d, J = 9.0 Hz, 1H), 7.68 (d, J = 9.0 Hz, 1H); MS, m/z (abundance), 2*E*/2*Z*: 306 (M^+ , 100%), 287 (17%), 271 (13%), 246 (74%), 228 (40%), 208 (31%), 196 (65%), 149 (4%). Anal. ($C_{15}H_9F_3N_2O_2$) C, H, N.

5.1.2.4. 5-[2*Z*-(4-Nitrophenyl)ethenyl]- N^1 -oxidebenzo[1,2-*c*]1,2,5-oxadiazole (14). Yellow solid (78 mg, 46%); mp 126.0–128.5 °C; IR ν_{max} 1613, 1525, 1343, 858, 613 cm^{-1} ; 1H NMR ($CDCl_3$, 400 MHz): δ 6.99 (d, J = 12.3 Hz, 1H), 7.05 (d, J = 12.3 Hz, 1H), 7.19 (br s, 1H), 7.49 (br s, 2H), 7.61 (d, J = 8.6 Hz, 2H), 8.18 (d, J = 8.6 Hz, 2H); ^{13}C NMR ($CDCl_3$, 100 MHz): δ 124.29, 130.57, 131.29, 132.14, 143.43, 147.57; MS, m/z (abundance), 2*Z*: 283 (M^+ , 100%), 267 (4%), 223 (32%), 179 (12%), 149 (3%). Anal. ($C_{14}H_9N_3O_4$) C, H, N.

5.1.2.5. 5-[2*Z*-(4-Nitrophenyl)ethenyl]benzo[1,2-*c*]1,2,5-oxadiazole (15). A mixture of 14 (100 mg, 0.4 mmol), Ph_3P (93 mg, 0.4 mmol), and EtOH (30.0 mL) as solvent was heated at reflux for 2 h. The EtOH was evaporated under reduced pressure. The residue was washed with petroleum ether to eliminate the

non-reacted Ph_3P and then purified by column chromatography (SiO_2 , petroleum ether/EtOAc (0–10%)), yielding derivative 15 as a yellow solid (88 mg, 82%); mp 143.6–145.1 °C; IR ν_{max} 1593, 1537, 1342, 856, 625 cm^{-1} ; 1H NMR ($CDCl_3$, 400 MHz): δ 6.88 (d, J = 12.4 Hz, 1H), 6.92 (d, J = 12.4 Hz, 1H), 7.15 (d, J = 9.3 Hz, 1H), 7.41 (d, J = 8.6 Hz, 2H), 7.69 (d, J = 9.0 Hz, 1H), 7.71 (s, 1H), 8.15 (d, J = 8.6 Hz, 2H); ^{13}C NMR ($CDCl_3$, 100 MHz): δ 116.24, 116.80, 124.30, 130.18, 131.72, 132.15, 133.33, 140.01, 143.09, 147.67, 148.75, 149.69; MS, m/z (abundance): 267 (M^+ , 26%), 250 (54%), 220 (17%), 190 (100%), 176 (6%). Anal. ($C_{14}H_9N_3O_3$) C, H, N.

5.2. Biology

Trypanosoma cruzi epimastigotes (Tulahuen 2 strain) were grown at 28 °C in an axenic medium (BHI-Tryptose) as previously described,¹⁵ complemented with 5% fetal calf serum. Cells from a 10-day-old culture (stationary phase) were inoculated into 50 mL of fresh culture medium to give an initial concentration of 1×10^6 cells/mL. Cell growth was followed by measuring everyday the absorbance of the culture at 600 nm. Before inoculation, the media were supplemented with the indicated amount of the drug from a stock solution in DMSO. The final concentration of DMSO in the culture media never exceeded 0.4% and the control was run in the presence of 0.4% DMSO and in the absence of any drug. No effect on epimastigote growth was observed by the presence of up to 1% DMSO in the culture media. To determine IC_{50} values, 50% inhibitory concentrations, parasite growth was followed in the absence (control) and presence of increasing concentrations of the corresponding drug. At day 5, the absorbance of the culture was measured and related to the control. The IC_{50} value was taken as the concentration of drug needed to reduce the absorbance ratio to 50%.

5.3. Crystallography study

The molecular structure of derivative 18, $C_7H_5N_3O_3$, was determined by X-ray diffraction methods. The diffraction pattern was collected at 120 K on an Enraf-Nonius KappaCCD diffractometer employing graphite mono-chromate $MoK\alpha$ radiation, and φ and ω scans to explore the reciprocal space. Data were collected with the program COLLECT^{27a} and reduced with DENZO and SCALEPACK.^{27b} The compound crystallizes in the monoclinic P21/*c* space group, with a = 7.012(1), b = 15.812(1), c = 7.453(1) Å, β = 112.85(1)°, and Z = 4. The structure was solved by direct^{27c} and Fourier^{27d} methods from 1517 reflections with $I > 2\sigma(I)$ and refined to an agreement R1-factor of 0.051. All hydrogen atoms, except for the hydroxyl one, were positioned stereo-chemically and refined with the riding model. The hydroxyl H-atom was refined isotopically with the O–H bond distance restrained to a target value of 0.82(1) Å. Intra-molecular bond distances and angles, along with other crystallographic data, are given as Supporting Information. The structure of compound 18 has been deposited in the Cambridge Crystallographic Data Centre, reference number CCDC-245371.

5.4. Structure–activity studies

5.4.1. 3D-QSAR. All CoMFA studies were performed on a Silicon Graphics O2 workstation. Structural manipulations were performed using SYBYL 6.9 with standard Tripos force field.^{20a} Three-dimensional structures used in the study were built using crystallographic data of derivative **18** (see Supporting Information)²³ and geometry was minimized using the Powell method until a root mean square (rms) gradient of 0.001 kcal/mol Å was obtained. All the compounds were built as the 6-substituted tautomers and as *E*-isomers (except for derivative **14**). Minimum energy geometries were obtained using the Powell method until a rms deviation of 0.001 kcal/mol Å was achieved. Partial atomic charges required for calculation of the electrostatic interaction were computed by the semi-empirical molecular orbital method²⁸ using the MOPAC program.²⁰ Charges were computed using the MNDO method. The net charge of derivatives was assigned as 0 e.u. Derivative **23** was used as template molecule. The steric and electrostatic potential fields for CoMFA were calculated at each lattice intersection of a regularly spaced grid of 2.0 Å. The lattice was defined automatically and is extended 4 Å units past van der Waals volume of all the molecules in *X*, *Y*, and *Z* directions. The van der Waals potential (Lennard-Jones) and columbic term, which represent, respectively, steric and electrostatic fields, were calculated using the Tripos force field. An sp^3 carbon atom with van der Waals radius of 1.52 Å and +1.0 charge served as the probe atom to calculate steric and electrostatic fields. The steric and electrostatic contributions were truncated as indicated in Table 4, and the electrostatic contributions were ignored at lattice intersections with maximum steric interactions. Indicator variables and $cLogP$ were used with the column filtering value (σ) of 2.0. The partial-least-squares (PLS)²⁹ method was used to derive a linear relationship between the biological activities and the molecular fields. Leave-one-out cross-validation with 2 kcal/mol column filtering was performed by omitting from the analysis those columns (lattice points) with an energy variance less than 2.0 kcal/mol. This allowed the determination of the optimum number of components associated with the lowest standard error of prediction. Lipophilic properties of the compounds were included into the analyses, as $cLogP$ ($LogP$ calculated by Ghose-Crippen method).²¹

5.4.2. Study of substituent α -atom. The compounds were built with standard bond lengths and angles using the Spartan'04, 1.0.1 version, suite of programs and energy-minimized by the molecular mechanics (MM) methods (using SYBYL molecular mechanics force fields implemented in Spartan'04 package).²¹ On the more flexible molecules we performed the corresponding conformational analysis using the MM methods (Conformational Distribution module implemented in Spartan'04 package). All the compounds were built as the 6-substituted tautomers and as *E*-isomers (except for derivative **11**). The geometry of the more stable conformations obtained by MM was fully optimized at the RHF level using MNDO semiempirical hamiltonian in the gas phase. Angles and bond lengths of compound

18 were compared with crystallographic data of **18** to validate the geometries optimization. The orbital population analysis was obtained through a single point calculation using the density functional methodology (Becke's exchange functional (B) and Becke's three-parameter adiabatic connection (B3) hybrid exchange functional were used in combination with the Lee-Yang-Parr correlation functional).²⁵ The standard 6-31G* basis set of DZP quality was used for orbital expansion to solve the Kohn-Sham equations for first- and second-row elements. For heavier atoms a pseudo-potential base (LACVP*) was used.

Acknowledgments

Financial support from CSIC-UdelaR and PEDECIBA is acknowledged. The authors thank PROSUL-CNPq (Brazil) for a scholarship to MB. OEP and EEC thank CONICET-Argentina and FAPESP-Brazil.

Supplementary data

Crystallographic data for derivative **18**. Supplementary data associated with this article can be found, in the online version, at [doi:10.1016/j.bmc.2005.07.072](https://doi.org/10.1016/j.bmc.2005.07.072)

References and notes

- <http://www.who.int/ctd/chagas>.
- (a) Cohen, J. E.; Tsai, E. C.; Ginsberg, H. J.; Godes, J. *Surg. Neurol.* **1998**, *49*, 324; (b) Carnerio-Proietti, A. B. F.; Lima-Martins, M. V. C.; Passos, V. M. A.; Carmo, R. A.; Pinheiro, S. R.; Rocha, P. R. M.; Proietti, F. A. *Haemophilia* **1998**, *4*, 47; (c) Pérez Ramírez, L.; Barnabe, C.; Sartori, A. M.; Ferreira, M. S.; Tolezano, J. E.; Nunes, E. V.; Burgarelli, M. K.; Silva, A. C.; Shikanai Yasuda, M. A.; Lima, J. N.; Da Cruz, A. M.; Oliveira, O. C.; Guilherme, C.; Bastrenta, B.; Tibayrenc, M. *Am. J. Trop. Med. Hyg.* **1999**, *61*, 198; (d) Concetti, H.; Retequi, M.; Pérez, G.; Pérez, H. *Hum. Pathol.* **2000**, *31*, 120; (e) Corti, M. *AIDS Patient Care STDS* **2000**, *14*, 581.
- Cerecetto, H.; González, M. *Curr. Top. Med. Chem.* **2002**, *2*, 1185.
- (a) Cerecetto, H.; Di Maio, R.; Ibarruri, G.; Seoane, G.; Denicola, A.; Quijano, C.; Peluffo, G.; Paulino, M. *Farmaco* **1998**, *53*, 89; (b) Di Maio, R.; Cerecetto, H.; Seoane, G.; Ochoa, C.; Arán, V. J.; Pérez, E.; Gómez-Barrio, A.; Muelas, S. *Arzneim.-Forsch. (Drug Res.)* **1999**, *49*, 759; (c) Cerecetto, H.; Di Maio, R.; González, M.; Risso, M.; Sagrera, G.; Seoane, G.; Denicola, A.; Peluffo, G.; Quijano, C.; Stoppani, A. O. M.; Paulino, M.; Olea-Azar, C.; Basombrio, M. A. *Eur. J. Med. Chem.* **2000**, *35*, 343; (d) Muelas, S.; Di Maio, R.; Cerecetto, H.; Seoane, G.; Ochoa, C.; Escario, J. A.; Gómez-Barrio, A. *Folia Parasitol.* **2001**, *48*, 105; (e) Martínez-Merino, V.; Cerecetto, H. *Bioorg. Med. Chem.* **2001**, *9*, 1025; (f) Paulino, M.; Iribarne, F.; Hansz, M.; Vega, M.; Seoane, G.; Cerecetto, H.; Di Maio, R.; Caracelli, I.; Zukerman-Schpector, J.; Olea, C.; Stoppani, A. O. M.; Berriman, M.; Fairlamb, A. H.; Tapia, O. *J. Mol. Struct. (Theochem.)* **2002**, *584*, 95; (g) Olea-Azar, C.; Rigol, C.; Mendizabal, F.; Morello, A.; Maya, J. D.; Moncada, C.; Cabrera, E.; Di Maio, R.; González, M.; Cerecetto, H. *Free Radical. Res.* **2003**, *37*,

- 993; (h) Aguirre, G.; Cabrera, E.; Cerecetto, H.; Di Maio, R.; González, M.; Seoane, G.; Duffaut, A.; Denicola, A.; Gil, M. J.; Martínez-Merino, V. *Eur. J. Med. Chem.* **2004**, *39*, 421; (i) Aguirre, G.; Boiani, M.; Cerecetto, H.; Gerpe, A.; González, M.; Fernández Sainz, Y.; Denicola, A.; Ochoa de Ocariz, C.; Nogal, J. J.; Montero, D.; Escario, J. A. *Arch. Pharm.* **2004**, *337*, 271; (j) Aguirre, G.; Boiani, L.; Cerecetto, H.; Fernández, M.; González, M.; Denicola, A.; Otero, L.; Gambino, D.; Rigol, C.; Olea-Azar, C.; Faundez, M. *Bioorg. Med. Chem.* **2004**, *12*, 4885; (k) Arán, V. J.; Ochoa, C.; Boiani, L.; Buccino, P.; Cerecetto, H.; Gerpe, A.; González, M.; Montero, D.; Nogal, J. J.; Gómez-Barrio, A.; Azqueta, A.; López de Cerain, A.; Piro, O. E.; Castellano, E. E. *Bioorg. Med. Chem.* **2005**, *13*, 3197.
5. (a) Cerecetto, H.; Di Maio, R.; González, M.; Risso, M.; Saenz, P.; Seoane, G.; Denicola, A.; Peluffo, G.; Quijano, C.; Olea-Azar, C. *J. Med. Chem.* **1999**, *42*, 1941; (b) Aguirre, G.; Cerecetto, H.; Di Maio, R.; González, M.; Porcal, W.; Seoane, G.; Denicola, A.; Ortega, M. A.; Aldana, I.; Monge, A. *Arch. Pharm.* **2002**, *335*, 15(c) See accompanying paper.
 6. (a) Olea-Azar, C.; Rigol, C.; Mendizabal, F.; Briones, R.; Cerecetto, H.; Di Maio, R.; Risso, M.; González, M.; Porcal, W. *Spectrochim. Acta A* **2003**, *59*, 69; (b) Olea-Azar, C.; Rigol, C.; Opazo, L.; Morello, A.; Maya, J. D.; Repetto, Y.; Aguirre, G.; Cerecetto, H.; Di Maio, R.; González, M.; Porcal, W. *J. Chin. Chem. Soc.* **2003**, *48*, 77.
 7. Cramer, R. D.; Patterson, D. E.; Bunce, J. J. *Am. Chem. Soc.* **1988**, *110*, 5959.
 8. (a) Harris, R. K.; Katritzky, A. R.; Oksne, S.; Bailey, A. S.; Paterson, W. G. *J. Chem. Soc.* **1963**, 197; (b) Boulton, A. J.; Katritzky, A. R.; Sewell, M. J.; Wallis, B. *J. Chem. Soc. B* **1967**, *9*, 914; (c) Boulton, A. J.; Halls, P. J.; Katritzky, A. R. *J. Chem. Soc. B* **1970**, 636; (d) Gasco, A.; Boulton, A. J. *Furoxans and Benzofuroxans In Advances in Heterocycles Chemistry*; Katritzky, A. R., Boulton, A. J., Eds.; J. Wiley: New York, 1981; Vol. 29, pp 251–340.
 9. (a) Gasco, A. M.; Ermondi, G.; Fruttero, R.; Gasco, A. *Eur. J. Med. Chem.* **1996**, *31*, 3; (b) Visentin, S.; Amiel, P.; Fruttero, R.; Boschi, D.; Roussel, C.; Giusta, L.; Carbone, E.; Gasco, A. *J. Med. Chem.* **1999**, *42*, 1422; (c) Ermondi, G.; Visentin, S.; Boschi, D.; Fruttero, R.; Gasco, A. *J. Mol. Struct.* **2000**, *523*, 149.
 10. (a) Boyer, J. H.; McCane, D. I.; McCarville, W. J.; Tweedie, A. T. *J. Am. Chem. Soc.* **1953**, *75*, 5298; (b) Boyer, J. H.; Schoen, W. *J. Am. Chem. Soc.* **1956**, *78*, 423.
 11. Boulton, A. J.; Ghosh, P. B.; Katritzky, A. R. *J. Chem. Soc. C* **1966**, 971.
 12. (a) Latham, D. W. S.; Meth-Cohn, O.; Suschitzky, H. *Tetrahedron Lett.* **1972**, *13*, 5365; (b) Latham, D. W. S.; Meth-Cohn, O.; Suschitzky, H. *J. Chem. Soc., Perkin Trans. I* **1976**, 2216.
 13. Boden, R. M. *Synth. Commun.* **1975**, 784.
 14. (a) Howard, E.; Olszewski, W. F. *J. Am. Chem. Soc.* **1959**, *81*, 1483; (b) Boyer, J. H.; Ellzey, S. E. *J. Org. Chem.* **1961**, *26*, 4684.
 15. Rubbo, H.; Denicola, A.; Radi, R. *Arch. Biochem. Biophys.* **1994**, *308*, 96.
 16. (a) Hansch, C.; Leo, A. *Exploring QSAR Fundamentals and Applications in Chemistry and Biology*; American Chemical Society: Washington, 1995; (b) Hansch, C.; Leo, A.; Hoekman, D. *Exploring QSAR. Hydrophobic Electronic and Steric Constants*; American Chemical Society: Washington, 1995.
 17. Lepper, E. R.; Ng, S. S. W.; Gütschow, M.; Weiss, M.; Hauschildt, S.; Hecker, T. K.; Luzzio, F. A.; Eger, K.; Figg, W. D. *J. Med. Chem.* **2004**, *47*, 2219.
 18. Squared correlation matrix of descriptors used in the 2D-QSAR study.

I₆	1			
MR	0.010	1		
F	0.2439	0.019	1	
I_{HBD}	0.017	0.0493	0.0001	1
r²	I₆	MR	F	I_{HBD}
 19. (a) Myers, R. H. *Classical and Modern Regression with Application*; PWS Publishers: Boston, 1986; (b) Daniel, C.; Wood, F. S. *Fitting Equations to Data*, 2nd ed.; Wiley: New York, 1980; (c) Draper, N. R.; Smith, H. *Applied Regression Analysis*, 2nd ed.; Wiley: New York, 1981.
 20. (a) SYBYL, Tripos Associates, 1699 South Hanley Road, Suite 303, St. Louis, Missouri 63144; (b) Clark, M.; Cramer, R. D., III; Van Opdenbosh, N. *J. Comput. Chem.* **1989**, *10*, 982.
 21. (a) Spartan'04; Wavefunction, Inc. 18401 Von Karman Avenue, Suite 370. Irvine, California 92612, USA.; (b) PC SPARTAN Pro User's Guide, Wavefunction Inc., California, 1999.
 22. Boehm, M.; Stuerzebecher, J.; Klebe, G. *J. Med. Chem.* **1999**, *42*, 458.
 23. (a) Johnson, C. K. ORTEP-II. A Fortran Thermal-Ellipsoid Plot Program. Report ORNL-5138, Oak Ridge National Laboratory, Tennessee, USA, 1976.; (b) The molecular skeleton is nearly planar (rms deviation of atoms from the mean plane equal to 0014 Å) with the hydroxyl H-atom also lying near the plane. The heterocycle presents essentially bonding asymmetry imposed by the NO group [$d(\text{N}_1\text{--O}_2) = 1436(2)$ Å $d(\text{N}_2\text{--O}_2) = 1382(2)$ Å]. The crystal is stabilized by an intermolecular H-bond involving the hydroxyl group of a molecule and the pendant arm nitrogen atom of other symmetry related molecule [$d(\text{H} \cdots \text{N}3') = 2050$ Å $\angle(\text{O}3\text{--H} \cdots \text{N}3') = 1464^\circ$].
 24. Ifa, D. R.; Rodrigues, C. R.; de Alencastro, R. B.; Fraga, C. A. M.; Barreiro, E. J. *J. Mol. Struct. (Theochem.)* **2002**, *505*, 11.
 25. (a) Becke, A. D. *Phys. Rev. A* **1988**, *38*, 3098; (b) Becke, A. D. *J. Chem. Phys.* **1993**, *56*, 5648; (c) Lee, C.; Yang, W.; Parr, R. G. *Phys. Rev. B Condens. Matter* **1988**, *37*, 785.
 26. (a) Cerecetto, H.; Dias, E.; Di Maio, R.; González, M.; Pacce, S.; Saenz, P.; Seoane, G.; Suescun, L.; Mombrú, A.; Fernández, G.; Lema, M.; Villalba, J. *J. Agric. Food Chem.* **2000**, *48*, 2995; (b) Boiani, M.; Cerecetto, H.; González, M.; Risso, M.; Olea-Azar, C.; Piro, O. E.; Castellano, E. E.; López de Cerain, A.; Ezpeleta, O.; Monge-Vega, A. *Eur. J. Med. Chem.* **2001**, *36*, 771.
 27. (a) Enraf-Nonius (1997–2000). COLLECT. Nonius B. V., Delft, The Netherlands. (b) Otwinowski, Z.; Minor, W. In *Methods in Enzymology*; Carter, C. W., Jr, Sweet, R. M., Eds.; Academic Press: New York, 1997, pp 307–326; (c) Sheldrick, G. M. *SHELXS-97. Program for Crystal Structure Resolution*; University of Göttingen: Göttingen, Germany, 1997; (d) Sheldrick, G. M. *SHELXL-97. Program for crystal structures analysis*; University of Göttingen: Göttingen, Germany, 1997.
 28. (a) Hehre, W. J.; Radom, L.; Schleyer, P. v. R.; Pople, J. A. *Ab Initio Molecular Orbital Theory*; Wiley: New York, 1986; (b) Hehre, W. J.; Shusterman, A. J.; Huang, W. W. *A Laboratory Book of Computational Organic Chemistry*; Wavefunction: California, 1996.
 29. Clark, M.; Cramer, R. D., III *Quant. Struct.-Act. Relat.* **1993**, *12*, 137.